A systematical study of the overall influence of carbon allotrope additives on performance, stability and redispersibility of magnetorheological fluids

Martin Cvek,[a,b*] *Miroslav Mrlik,*[a] *Robert Moucka,*[a] *Michal Sedlacik*[a]

[a] Centre of Polymer Systems, University Institute, Tomas Bata University in Zlín, Trida T. Bati 5678, 760 01 Zlín, Czech Republic

[b] Polymer Centre, Faculty of Technology, Tomas Bata University in Zlín, Vavreckova 275, 760 01 Zlín, Czech Republic

Abstract. To this date many different additives have been used in order to stabilize the magnetorheological fluids or to enhance their performance, but their ranking in terms of the efficiency is still lacking. To design the efficient magnetorheological fluid it is necessary to analyze the overall effects of the additives on its complex behavior. In this study, carbon allotropes – fullerene powder, carbon nanotubes, graphene nanoplatelets – were added into the carbonyl iron-based magnetorheological fluids to examine their effect on stability and utility properties. The magnetorheological behavior of designed mixtures was investigated and obtained experimental data were numerically evaluated using the Robertson–Stiff model. While the fine fullerene powder acted as a gap-filler reinforcing field-induced structures, the other additives employed rather disrupted the microstructure during the shear. The role of the additives during the formation of field-induced structures was pointed out. The sedimentation stability was examined using Turbiscan analyzer as well as by direct observation method. Both approaches revealed that the carbon nanotubes possessed the highest stabilization effect. Carbon nanotubes also most effectively prevented packing the iron microparticles into a stiff sediment as was confirmed via redispersibility measurements.

[*]Corresponding author. Tel: 420 732 122 529. E-mail: cvek@utb.cz

Keywords: magnetorheology; additive; graphene; suspension stabilization; redispersibility; modeling

1. Introduction

Magnetorheological fluids (MRFs) are a type of field-responsive system composed of micron-sized magnetic particles dispersed in a non-magnetic medium. Such systems exhibit Newtonian-like behavior in the absence of magnetic field, but in a fraction of a millisecond they solidify when an external magnetic field is applied. The field-induced transformation of their rheological properties known as magnetorheological (MR) effect is tunable and reversible. This phenomenon is based on the polarization of the particles that consequently attract each other resulting in rigid chain/column-like particle structures which span the flow domain [1-3]. These unique features make the MRFs suitable for applications in vibration dampers [4] and shock absorbers [5], clutches [6], brakes [7] or polishing devices [8].

As a dispersed phase, the carbonyl iron (CI) particles are considered to be suitable candidates for MRF preparation due to their appropriate size, high saturation magnetization, and low hysteresis. However, high density of the CI compared to disperse medium causes serious sedimentation issues [3, 9].

To overcome this drawback, various strategies have been proposed involving the modification of the CI surface with various polymers (even electrically-conductive polymers) [9, 10], inorganics [11] or self-assembled monolayers [12]. The modification layer can be fabricated via a number of methods. The simple dispersion polymerization [13] or emulsion polymerizations [14] belong to the early methods used. More advanced techniques such as atom transfer radical polymerization [9, 15] or reversible addition fragmentation chain transfer and

click chemistry [16] allowing the control of grafting layer at molecular level were used to precisely control the final properties of the particles and consequently the behavior of the MRFs. In the recent work, Choi et al. [17] utilized a supercritical carbon dioxide as a physical foaming agent to tune the properties of grafted layer onto the magnetic particles. Generally, all the mentioned approaches enhanced utility properties and practical applicability of the MRFs to a certain degree. However, the application of the modifying layers can be time consuming, involves problematic large-scale production and often requires the use of environmentally harmful chemicals.

Use of additives in the MRFs is a well-known approach to enhancement of performance and stability properties of the MRFs. This approach is straightforward, hence effective and no special or toxic chemicals are needed, thus it appears to be beneficial also from the environmental point of view. The incorporated additives are mostly submicron-sized gap-fillers that occupy the interspaces between the magnetic particles reducing their sedimentation rate while increasing the dispersion stability [3, 18]. The diverse additives including fumed silica [19], organoclays [20], γ-Fe_2O_3 nanoparticles [21], graphene oxide [3] *etc*. were utilized in the MRFs for mentioned enhancing effects. Recent study [22] further investigates the effect of non-magnetic rod-like ferrous oxalate dihydrate particles and their magnetic iron oxide rod-like analogues on the MR effect and stability properties.

Obviously, the materials of different elemental compositions, and different shapes [3, 9, 23, 24] (spherical, rod-like/fibrous, plate-like) were used as additives for the MRFs. Based on the literature survey, it is also important to mention that the MRFs containing the additives were tested under different conditions (particle/additive ratio, dispersion medium, applied magnetic field) thus the genuine effect of the individual additives is not easy to compare, since the studies were carried out and evaluated differently. In other words, the comparison of the overall efficiency of the employed additives is still unclear.

The aim of this study was to investigate the influence of different additives on the performance of the MRFs under the representative conditions. The chosen additives were based on different carbon allotropes of various morphologies, which were represented by fullerene (C_{60}) powder, carbon nanotubes (CNTs), and graphene nanoplatelets (GNPs). The MR performance of as-designed MRFs was assessed by the evaluation of their rheological data using the Robertson–Stiff (R–S) model, which appears to be a better alternative and more reliable tool to describe rheological data of the MRFs in the steady shear regime, when compared to the conventional Herschel–Bulkley model [25]. The effect of additives on the toughness of the induced particle structures was examined using magneto-oscillatory measurements. Finally, the sedimentation stability and redispersibility of the MRFs as the important factors influencing their practical effectivity [19, 26] were investigated and compared.

2. Materials and Methods

2.1 ***Materials.*** The carbonyl iron (CI) particles (SL grade; BASF, Germany) and silicone oil (SO) (Lukosiol M200, Chemical Works Kolín, Czech Republic; dynamic viscosity of 197 mPa·s, density of 0.97 g·cm^{-3} at 25 °C) were used as a dispersed phase and a suspending medium, respectively, for a preparation of MRFs. The additives were represented by fine fullerene powder (C_{60}; 99.5%, density of 1.65 g·cm^{-3}), multi-walled carbon nanotubes (CNTs; > 90% carbon basis, diameter of 110–170 nm; length of 5–9 μm, density of 1.70 g·cm^{-3}), and graphene nanoplatelets powder (GNPs; density of 1.90 g·cm^{-3}) – all obtained from Sigma (Sigma–Aldrich, USA). All materials were used as received, fullerenes were gently ground into fine powder using a pestle and mortar.

2.2 ***Microscopy characterization of the particles.*** The morphology observations of the CI particles and the employed additives were performed on a field-emission scanning electron microscope (SEM) (FEI, Nova NanoSEM 450, Japan). While the dimensions and morphology

of the CI particles were studied at 10 kV accelerating voltage in high vacuum mode, the SEM micrographs of the carbonaceous additives were taken in low vacuum mode using the Helix detector.

2.3 ***Preparation of MRFs.*** To prepare the MRFs, the CI particle content was fixed to 60 wt.% (~15.7 vol.%), while the amounts of 1 or 3 wt.% additives were introduced into the mixtures. The CI particles, SO, and the corresponding additive as the components of the MRFs were thoroughly mixed using a dispersing instrument Ultra Turrax T 10 standard (IKA® Werke, Germany) for 5 minutes and then sonicated for additional 2 minutes with the help of an ultrasonic device (K-12LE, Kraintek, Slovakia) to obtain well-dispersed systems. The temped bath was used to maintain the temperature of the samples at desired 25 °C during the sonication process. After the preparation, the MRFs were immediately characterized. The names of the samples are coded using a following key: MRF-*additive-amount of additive*.

2.4 ***Magnetorheological measurements.*** A rotational rheometer Physica (MCR502, Anton Paar GmbH, Austria) equipped with a magneto–device (Physica MRD 170/1T) was used to investigate the rheological properties of prepared MRFs. The gap size between the non-magnetic titanium plate (PP20/MRD/TI) geometry and the static steel plate was 0.5 mm, while 0.2 mL of MRF sample was injected between them. The steady shear experiments were performed in a control shear rate mode within the shear rate range of 0.01–250 s^{-1}. The electric current (0–1.5 A) generated using a power station (PS/MRD/5A) was correlated with true magnetic field (0–432 $kA \cdot m^{-1}$) perpendicular to the samples with a Teslameter (Magnet Physic, FH 51, Dr. Steingroever GmbH, Germany). The detailed measuring protocol of the steady shear investigations can be found in our previous study [25]. The rheological data were collected three times with freshly prepared samples in order to ensure repeatability and accuracy of the measurements. The average values of corresponding rheological quantities were calculated, used for the numerical evaluation and presented in rheograms. In addition, the response time of

the MRFs to magnetic field and reproducibility of the internal structure formation were investigated using the on/off tests. The condition in this characterization included a constant shear rate of 50 s^{-1}, while the field of 0 $kA \cdot m^{-1}$and 288 $kA \cdot m^{-1}$ was periodically applied in 60 s intervals.

Dynamic rheological tests based on amplitude sweeps under various magnetic fields were conducted. These experiments were performed in order to clarify the role of additives on the MRF behavior within the linear viscoelasticity region and beyond it. In the amplitude sweep, a sinusoidal stress at a constant frequency of 10 Hz with a strain amplitude in the range of 10^{-3}–10^{1} % was applied to the investigated sample and thus the storage modulus, *G'*, and the loss modulus, *G''*, dependences were obtained.

To impose the same initial conditioning before each test run, the MRF was pre-sheared at shear rate of 50 s^{-1} for 60 s. Moreover, the corresponding magnetic field was applied for 30 s before each on–state measurement in order to fully develop the field-induced structures in the system. All MR measurements were performed at a constant temperature of 25 °C maintained by a thermostatic unit (Julabo FS18, Germany).

2.5 ***Sedimentation stability.*** The stability of the MRFs can be determined using several approaches. Besides instrumented optical method [27], or direct observation [22, 28], also alternatives such as tensiometric [29] or inductance [30, 31] measurements can be successfully employed. In this study, Turbiscan® Lab (Formulaction, France) analyzer was used to investigate the sedimentation stability of testes samples. The instrument is equipped with two synchronous optical sensors that measure the transmitted and the backscattered (BS) near-infrared monochromatic light (λ = 880 nm), i.e. light which goes through the sample and light scattered backwards by the sample, respectively. In practice, the MRFs are placed in flat-bottomed cylindrical glass tubes (volume of 4 mL), while the detection head periodically scans a sample by moving vertically along the analysis cell and acquiring data every 40 μm. Due to

sample instability, the differences in transmitted, and BS signals versus time are recorded. The measurements were performed on freshly-dispersed samples at a constant temperature of 25 °C. Detailed description of Turbiscan® apparatus principle can be found elsewhere [32].

The long-term MRF stability was obtained performing the naked-eye observation method. The well-dispersed MRFs were transferred into cylindrical tubes (inner diameter of 13 mm, height of 48 mm) and the position of macroscopic phase boundary between the concentrated fraction and relatively clear oil-rich phase was recorded as a function of time [18]. The sedimentation ratio was expressed as a height of the particle-rich phase relative to the total MRF height. The advantages as well as drawbacks of both methods related to sedimentation stability were finally discussed.

2.6 ***Redispersibility.*** The redispersibility tests were performed on the basis of the ASTM-D5-05a standard, which was originally designed to determine the penetration of bituminous materials. Nevertheless, as shown elsewhere [11, 26] this concept can be also applied for MRFs testing. This testing method can be further modified for the MRFs' testing in repeated penetration/extraction steps as shown recently by Portillo et al. [33]. Herein, the M350-5 CT (Testometric Company, Lancashire, UK) device was used to execute the controlled motion of the standard needle at a desired velocity of 10 $mm \cdot min^{-1}$. The needle penetrated the MRF and the stiffness of the sediment, expressed as a force needed to overcome the needle buoyancy and to penetrate the sample, was recorded by an analytical balance (KERN KB 360-3N, Germany) with an accuracy of 1 mg (9.8×10^{-3} mN). The data were automatically read/collected by a computer. The representative MRFs were prepared by ultrasonic dispersing (Sonopuls HD 2070, Bandelin electronic, Germany) prior to their testing. All the experiments were carried out at laboratory conditions after 168-hour inactivity.

3. Results and discussion

3.1 ***Microstructure analysis.*** The size and morphology of the MRF components can remarkably affect the overall behavior of the MRFs, therefore the SEM was chosen as a suitable analytical tool to explore these characteristics. Figure 1 depicts the SEM micrographs of the employed MRFs particulate components. As seen, the CI particles were almost perfectly spherical with quite smooth surface and diameter in a range of 1–5 μm. The ground C_{60} powder exhibited irregular shapes with sharp edges and the grain size in sub-micron range similarly as in work by Zhao et al. [34]. The CNTs with a high aspect ratio developed self-entangled clusters, while the GNPs formed micron-size several layer-thick sheets. The obtained information about particle morphology is further discussed with the connection to tested MRF characteristics.

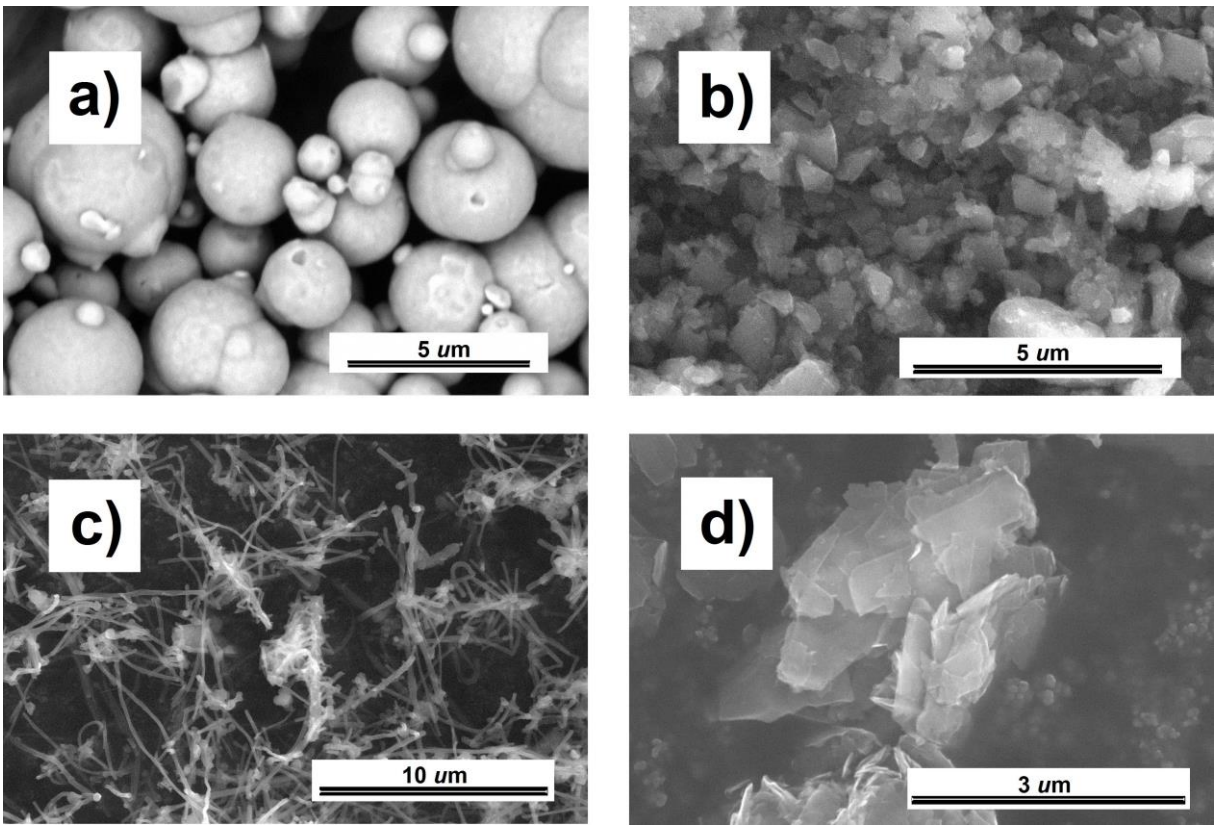

Figure 1. SEM images of the CI particles (*a*) and the carbonaceous additives, namely, fine C_{60} powder (*b*), CNTs (*c*), and GNPs (*d*).

3.2 ***Magnetorheological activity under steady shear.*** The performance of the MRFs in magnetic field is a crucial requirement for many engineering applications, therefore the steady shear measurements on formulated MRFs were performed and evaluated. In a shearing mode, the MR activity can be evaluated via different viscoplastic models among which, the most popular are the Bingham plastic, and the Herschel–Bulkley models. In our preceding study, we have shown that predictive/fitting capabilities of the R–S model are superior and thus this model can provide more accurate fits with the experimental data, which was also proven via statistical analysis [25]. The R–S model employing the parameters applicable for the MRFs has following form:

$$\tau = \left[K^{\frac{1}{n}} |\dot{\gamma}|^{\frac{n-1}{n}} + \left(\frac{\tau_0}{|\dot{\gamma}|} \right)^{\frac{1}{n}} \right]^n \dot{\gamma} \qquad (1)$$

where τ is the shear stress, the τ_0 is the yield stress controlled by the magnetic field strength (H), $\dot{\gamma}$ denotes the shear rate, while K and n are the consistency index and power–law exponent, respectively [25, 35].

3.2.1 ***Off-state evaluation.*** We compared the MR flow behavior of the MRFs with and without additives to examine their effect as shown in Figure 2. As seen, the presence of the additives at the amount as low as 1 wt.% influenced the MR characteristics.

Firstly, the attention was paid to the evaluation of the MRFs off-state flow behavior. The off-state τ generally increased due to the presence of the carbon additives, which was also observed elsewhere on nano-silica filler [36]. The off-state τ of the MRF-C_{60}-1 and MRF-GNP-1 was comparable with the τ of reference sample. On the other hand, the MRF-CNT-1 exhibited the highest increment of this quantity probably due to high-volume-to-surface ratio of the CNTs. Such trends were also confirmed and quantified via n parameter of the R–S model, which compares the flow behavior of the MRF with a Newtonian fluid. When n approaches 1, the

typical Newtonian behavior is obtained, while n value in the range of $0 < n < 1$ corresponds to shear thinning flow behavior. The n as a fitting parameter of the R–S model was close to 1 for the reference sample as well as MRF-C_{60}-1 and MRF-GNP-1, which is in accordance with the character of the obtained flow curves. The MRF-CNT-1 exhibited n equal to ~0.78 referring to more pronounced pseudoplasticity.

Figure 2 also shows the flow curves of the tested MRFs containing 3 wt.% of the additives. The presence of the higher amount of all additives further increased the off-state τ values when compared with the situation for the MRFs containing only 1 wt.% of the additives. Similar effect was observed by Zhang et al. [3] on various CI/graphene oxide mixtures with different ratios of the components. Again, this phenomenon was the most significant in the MRF-CNT-3, while remaining two systems almost preserved the original values of the reference system. These results were consistent with the numerical results (Table 1), as the MRF-C_{60}-3 and the MRF-GNP-3 exhibited n values around ~0.90, while in the MRF-CNT-3 the n was calculated to be only ~0.41 reflecting the severe pseudoplasticity of the system. All numerical results and fitting parameters are included in Table 1.

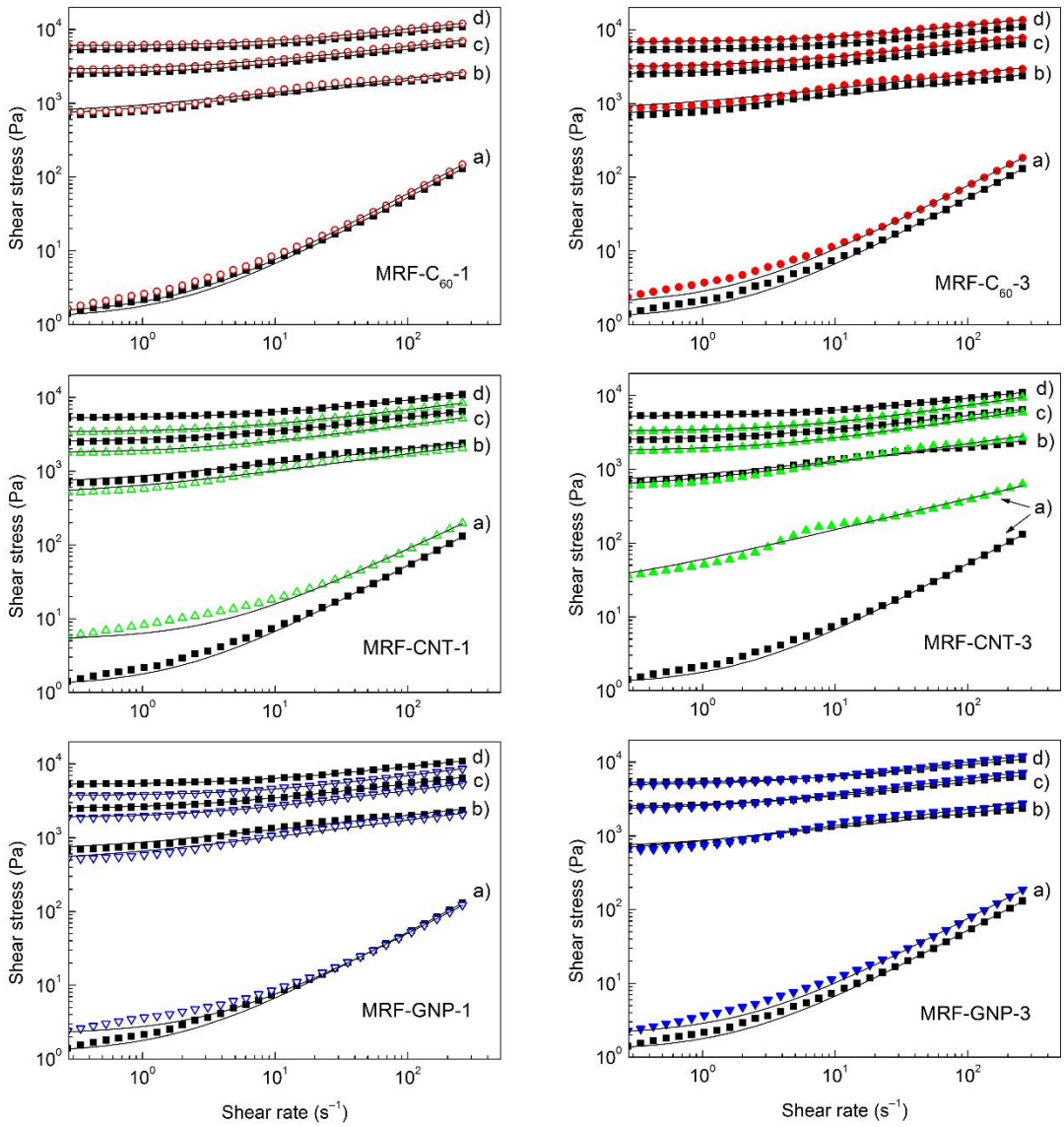

Figure 2. The shear stress vs. shear rate dependences for the reference sample (*solid squares*), and the MRFs containing 1 wt.% (*open symbols*) or 3 wt.% (*solid symbols*) of fine C_{60} powder (*circles*), the CNTs (*up-triangles*), or the GNPs (*down-triangles*) at the off-state (*a*), and at 144 (*b*), 288 (*c*), 432 kA·m^{-1} (*d*) magnetic field strengths. The solid lines refer to the R–S model predictions.

3.2.2 ***On-state evaluation.*** At the on-state, the significant increase of the τ values can be observed (Figure 2) due to the formation of chain-like structures spanning the geometry. Thus,

the MRFs possessed a solid-like behavior accompanied by breaking and reforming of the particle chains during the shear flow [24]. Interestingly, the MRF containing fine C_{60} powder exhibited slightly higher on-state τ values at corresponding magnetic fields when compared with the reference sample. This phenomenon was observed on different additives [3, 20, 37] and can be explained as a consequence of the gap-filling the interspaces among the CI particles with the nano-sized additives. Therefore, the fine C_{60} powder at such small amounts can enhance the contact of the CI particles resulting in more robust field-induced structures.

However, the effect of other carbonaceous additives on the performance of the MRF followed the opposite trends. The presence of CNTs and GNPs decreased the on-state τ values, while the former demonstrated also already mentioned notably increased off-state leading to lower efficiency of the system in terms of its relative MR performance. These additives reduced the contact between the CI particles due to their morphological structure (Figure 1) and caused decreased toughness of the internal particle chains, which fits well with the literature dealing with non-magnetic nano-additives [20, 37]. Admittedly, the CNTs were recently reported [38] as an additive enhancing the MR properties. However, the previous research was performed using the single-walled CNTs (purity of ~50%), which possessed certain magnetic properties even after purification process due to the residual iron catalyst resulting from the synthesis [38]. In this case the CNTs and GNPs underwent collisions with the CI chain-like structures and instead of the gap-filling effect they possess the weakening effect on the formation of induced structures due to their 2-dimensional structure. As seen in Table 1, this assertion is supported by numerical description obtained from empirical modeling. The *K* parameter of the R–S model physically reflects the rigidity of the particle internal structures as shown in our previous paper [25]. Thus, the trends in *K* parameter value confirm the hardening/weakening effects of the employed additives.

Table 1. Calculated R–S model parameters for the CI-based MRFs containing different amounts of the carbon additives under various magnetic field strengths.

Magnetic field	**0 kA·m^{-1}**	**72 kA·m^{-1}**	**144 kA·m^{-1}**	**216 kA·m^{-1}**	**288 kA·m^{-1}**	**360 kA·m^{-1}**	**432 kA·m^{-1}**
MRF (reference sample)							
τ_0	1.211	153.6	680.4	1489	2518	3787	5270
K	0.6102	250.6	818.3	1391	2034	2792	3735
n	0.9639	0.2362	0.1968	0.2077	0.2108	0.2059	0.1938
MRF-C$_{60}$-1							
τ_0	1.399	170.5	744.0	1667	2878	4363	6011
K	0.6880	288.9	898.5	1597	2350	3181	4107
n	0.9644	0.2245	0.1940	0.1977	0.2008	0.1994	0.1954
MRF-CNT-1							
τ_0	5.173	123.7	501.6	1088	1780	2560	3394
K	1.684	209.3	587.8	1016	1435	1951	2496
n	0.8534	0.2532	0.2327	0.2318	0.2340	0.2259	0.2171
MRF-GNP-1							
τ_0	2.193	117.2	506.2	1123	1874	2720	3751
K	0.6553	209.1	604.3	1040	1524	2010	2430
n	0.9371	0.2541	0.2296	0.2315	0.2273	0.2247	0.2265
MRF-C$_{60}$-3							
τ_0	1.895	204.6	846.5	1865	3147	4773	6839
K	1.101	336.3	1008	1775	2589	3566	4806
n	0.9195	0.2146	0.1987	0.2006	0.2028	0.1994	0.1885
MRF-CNT-3							
τ_0	24.59	149.2	587.7	1138	1800	2553	3327
K	57.10	362.2	688.3	1013	1324	1691	2090
n	0.4227	0.2359	0.2548	0.2626	0.2760	0.2766	0.2715
MRF-GNP-3							
τ_0	2.018	137.3	598.4	1322	2308	3463	4895
K	0.9475	277.3	820.5	1412	2107	2846	3725
n	0.9478	0.2475	0.2243	0.2263	0.2245	0.2213	0.2123

3.2.3 ***Yield stress evaluation.*** Despite an ongoing debate whether true τ_0 exists or not, the concept of τ_0 is very useful and desirable in many practical application, once it is properly defined and delineated [39]. This quantity is commonly determined using appropriate rheological models [40, 41]. Based on the numerical results, one can notice that studied MRFs exhibited small τ_0 even at the off-state. Similar phenomenon was observed elsewhere and was explained as a consequence of the particle aggregation [42]. Nevertheless, this can be expected

as some force is required to initiate deformation or flow of the MRFs even at the off-state. As we demonstrated, such small τ_0 can be determined when appropriate models are used.

The dependence of the dynamic τ_0 predicted according to the R–S model on the applied magnetic field strength is plotted in Figure 3. As seen, the data followed well-known magnetic-polarization model that predicts a relation between the field-dependent τ_0 and the strength of applied field [27]. The τ_0 increases with the exponent 2.0, when a weak magnetic field is imposed. At a certain magnetic field strength, known as critical magnetic field, H_C, the local particle saturation becomes apparent and the slope of the dependence decreases to 1.5 [43]. This transition behavior was apparent in all MRFs, while the H_C was found to be ~250 kA·m^{-1} as the nano-additives in such small amounts had a negligible effect on this quantity.

Generally, the fine C_{60} powder acted as the gap-filler among the CI micro-particles making the induced structures more rigid, while the other two additives involved disrupted the particle structures during the steady shearing in external magnetic field. The similar trend was observed when 3 wt.% of the nano-additives were employed, nevertheless the MRF-GNP-3 exhibited similar τ_0 as the reference, whereas the MRF-CNT-3 possessed slightly lower τ_0 especially at high magnetic field stregnths when compared with the reference. Comparing the data (Table 1), it can be noticed that the τ_0 values were interestingly higher when larger amounts of corresponding additives were incorporated. This phenomenon can be explained as follows: higher amount of additive results in lower relative portion of SO, which makes the MRF thicker and gives rise to the on-state values including the τ_0.

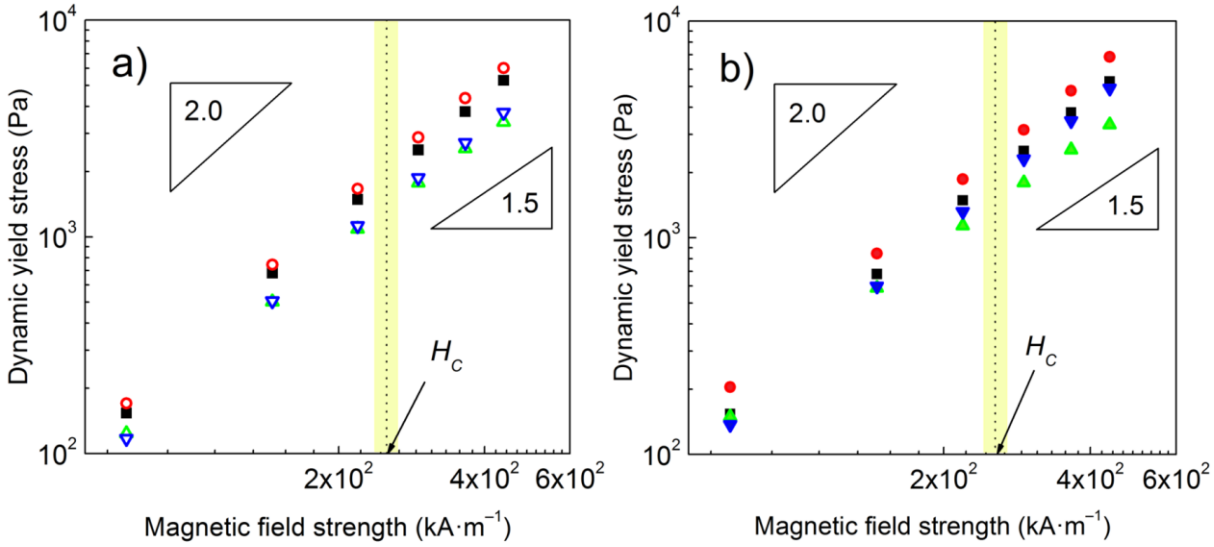

Figure 3. The dynamic yield stress vs. magnetic field strength dependences for the reference sample (*solid squares*), and the MRFs containing 1 wt.% (*a; open symbols*) or 3 wt.% (*b; solid symbols*) of fine C_{60} powder (*circles*), the CNTs (*up-triangles*), or the GNPs (*down-triangles*).

3.3 ***Magnetorheological activity under dynamic magnetic field.*** The important characteristics of the MR phenomenon such as very fast process rate and the reversibility were considered. The presence of non-magnetic additives might negatively affect the rate of the CI structure formation and possible destruction of certain brittle additives during repeatable shearing can induce problems with reproducibility of the process. As expected, the τ values followed similar trends as obtained in steady shear magnetorheology (Figure 2) and from obvious above-indicated reasons the presence of fine C_{60} powder slightly increased its value, while the MRFs containing other additives exhibited rather lower τ values. To address the repeatability in all the investigated MRFs, the repeatable on-state increase of τ values was followed by their decrease to original off-state values as seen in Figure 4. The process was generally characterized by an abrupt increase/decrease of the τ as a reaction on switching magnetic field thorough several operating cycles. The additives can be perceived as physical barriers acting against the CI particles' locomotion. Their presence however did not significantly affect the

rate of the structure formation as this process is driven by strong magnetic forces and the additives were incorporated in relatively low amounts. Generally, the key characteristics of the MR effect were sufficiently retained showing the potential of designed MRFs in practical MR devices.

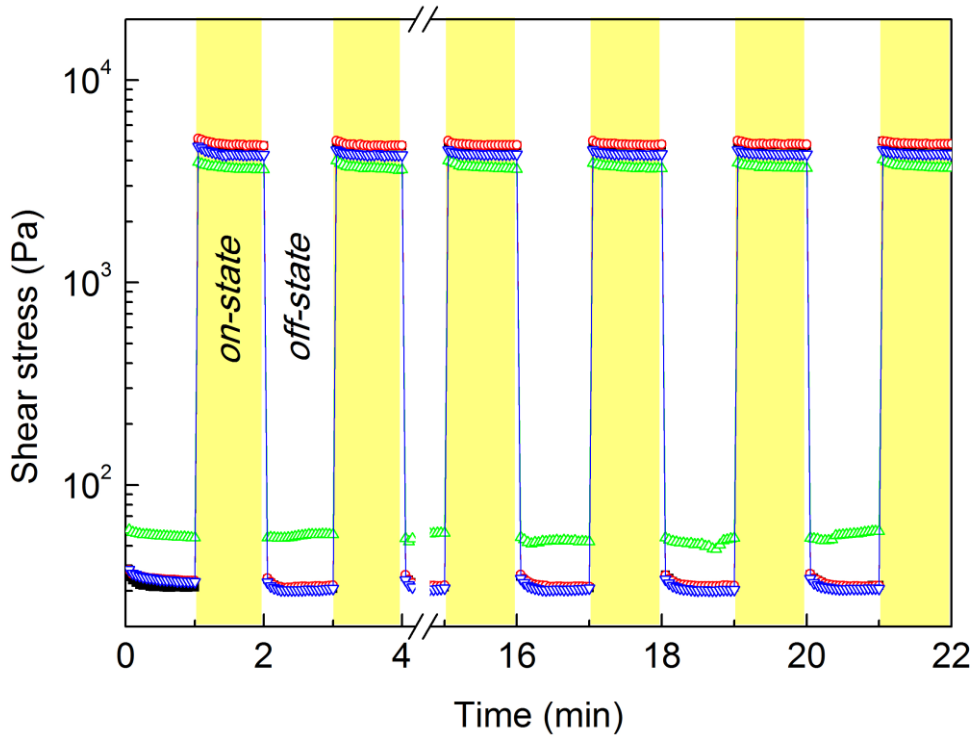

Figure 4. The shear stress vs. time dependences during periodically switching off/on magnetic field (~288 kA·m^{-1}) at a shear rate of 50 s^{-1} for the reference sample (*solid squares*), and the MRFs containing 1 wt.% of fine C_{60} powder (*open circles*), the CNTs (*open up-triangles*), or the GNPs (*open down-triangles*). The white/yellow regions refer to off/on states.

3.4 ***Dynamic magnetorheological properties.*** In order to explore the strength of the field-induced particle chains, the oscillatory tests comprising of amplitude sweeps under various magnetic field strengths were acquired. Analogously to magneto-steady shear, the presence of

applied magnetic field yielded the formation of chain-like structures resulting in an increase of both the *G'* and *G''*. As seen, all curves exhibited similar character and the onset of non-linearity manifested at relatively low strain amplitudes, similarly as obtained by other researchers [38]. Interestingly, the effects of additives during magneto-oscillatory-shear manifested in lower degree when compared to the situation under the magneto-steady shear, thus the differences in *G'* values were generally less pronounced when compared to the reference (Figure 5). To address this phenomenon, the mechanisms of the additives' action on the formation of the CI structures were proposed.

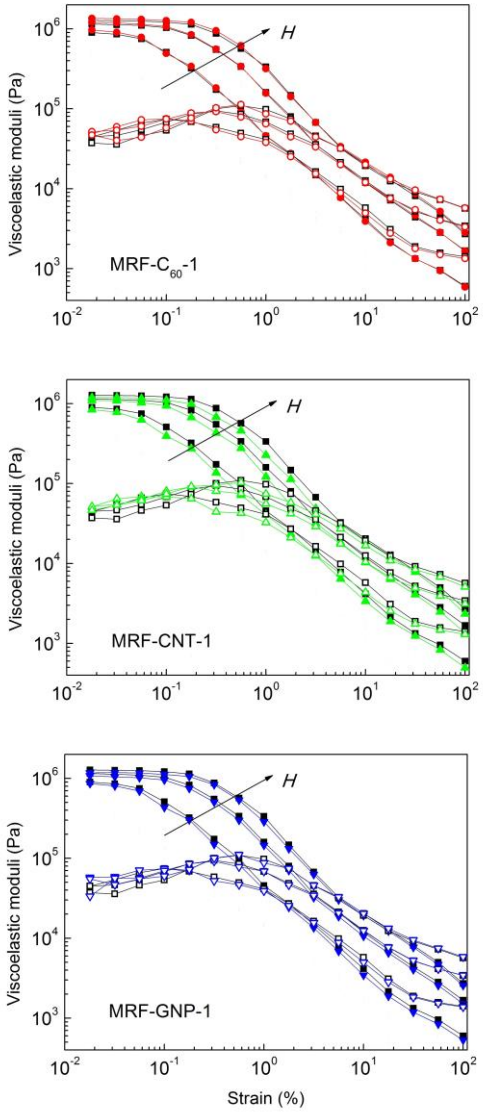

Figure 5. The storage (*solid symbols*) and the loss (*open symbols*) moduli vs. strain dependences for the reference sample (*squares*), and the MRFs containing 1 wt.% of fine C_{60} powder (*circles*), the CNTs (*up-triangles*), or the GNPs (*down-triangles*) under increasing magnetic field strength (144, 288, and 432 $kA \cdot m^{-1}$) denoted by the arrow.

3.5 ***Theoretical mechanisms of carbonaceous additives' action on the formation of the CI structures.*** As seen above (Figure 2), all tested additives increased the off-state τ of the MRFs as their presence increased frictional forces and the hydrodynamic volume [44]. However, the trend in the on-state rheological behavior varied based on the additive employed. As a sub-micron-sized material, fine C_{60} powder possessed a gap-filling effect based on the bridging the gaps among the adjacent CI particles and thereby enhancing the rigidity of the internal structures and MR properties (shear stress, yield stress) [27]. On the contrary, the presence of the CNTs and GNPs interrupted chain formation of the CI particles causing them less resistant against applied force. The situation was more pronounced under steady shear conditions when compared to small amplitude oscillatory shear. In the former case, the particles including the additives can rotate due to Couette flow velocity profile (Figure 6). The rotations can increase the hydrodynamic volume of the additives, which leads to higher distances between the CI particles lowering the magnetic dipole–dipole interactions and consequently the MR performance [13]. This feature was more pronounced for non-spherical additives such as CNTs and GNPs. Similar phenomena were observed in the literature dealing with the non-magnetic additives [3, 44] or even non-magnetic coatings [13, 28] applied on the CI particles' surface. The results suggest, that under the oscillatory shear the additives integrated the CI particle structures to higher degree leading to only slight decrease of *G'* values when compared to the reference. In this study, the most obvious effect was attributed to the presence of the CNTs,

which from a wider perspective showed their indisputable advantages for sedimentation stabilization purposes, as will be shown further in text.

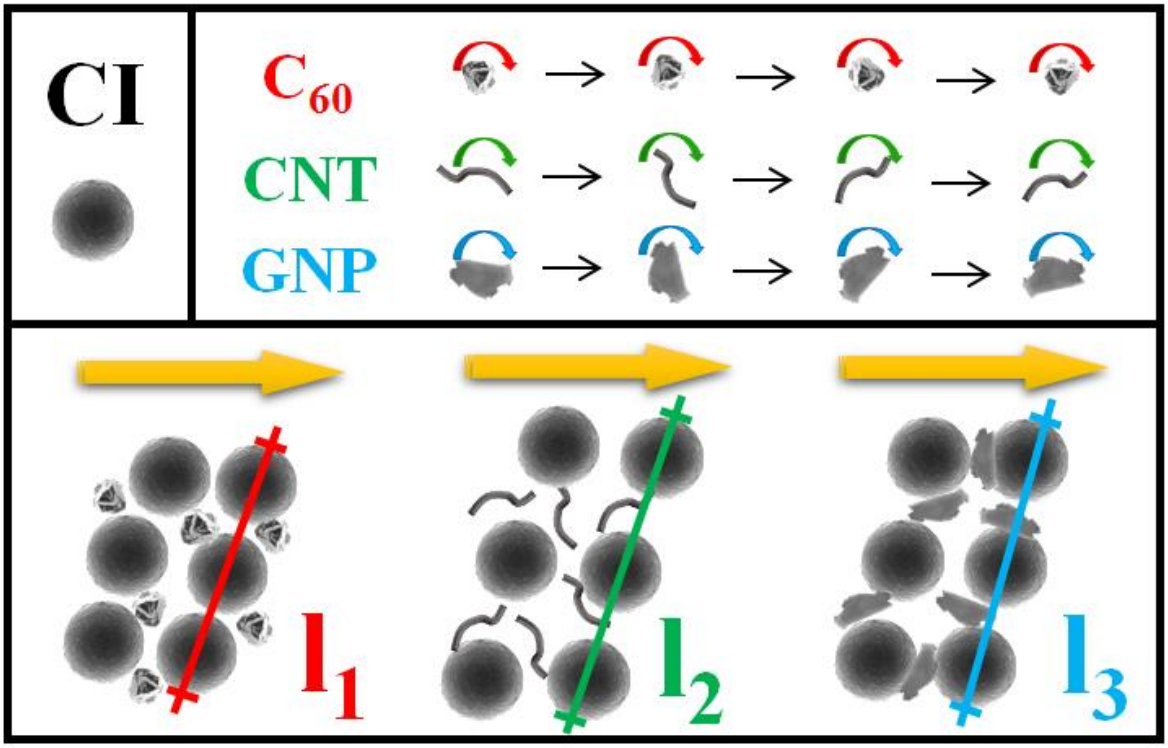

Figure 6. Schematic representation of fine C_{60} powder, CNTs and GNPs added into the CI-based MRF. The lines represent the average distance between three neighboring CI particles ($l_1 < l_3 < l_2$), which is related to the intensity of induced magnetic moments.

3.6 ***Sedimentation stability.*** The short-term sedimentation properties of the MRFs were investigated using an optical analyzer. In the principle, the instrument measures the BS signals, which vary with the cell height (Y-axis) over time [27]. Figure 7 displays Turbiscan profiles, in which the bottom of the sample is represented on the left-hand side of the graph, while the top of the sample corresponds to its right-hand side. The scanning is repeated over time, which is denoted by the color of the lines. Presented results are displayed in delta, Δ, mode, i.e. the first scan is subtracted from all other scans, which allows easier visualization of the variations.

As known, the occurrence of significant BS variation at the top of the spectra indicates the clarification phenomenon. The ΔBS decreases as the particles in the suspension sediment, and as a result the BS signal is lower. On the contrary, the changes at the bottom of the spectra denote developing sedimentation cake, and the BS signal increases due to locally increased concentration of the particles. The stability of the MRFs containing 1 wt.% of the carbon additives was evaluated. As seen in Figure 7, the reference sample and the MRF-C_{60}-1 displayed similar Turbiscan spectra regarding the position of the peaks and their intensity. However, in fact a broader clarification peak in the latter suspension indicated that a small amount of fine C_{60} powder slightly reduced stability of the suspension. The lowest BS variation exhibited MRF-CNT-1, which corresponded to the most stable MR system. The remarkable stability enhancement due to the presence of CNTs can be attributed to increased friction force as a result of their high specific surface area, which affects the MRF viscosity [45]. Finally, the presence of GNPs increased suspension stability to a certain degree, but not as significantly as the CNTs at the same amount. The Turbiscan spectra of the MRFs containing 3 wt.% of the carbon additives are included in electronic supplementary information (ESI) (please see Figure S1).

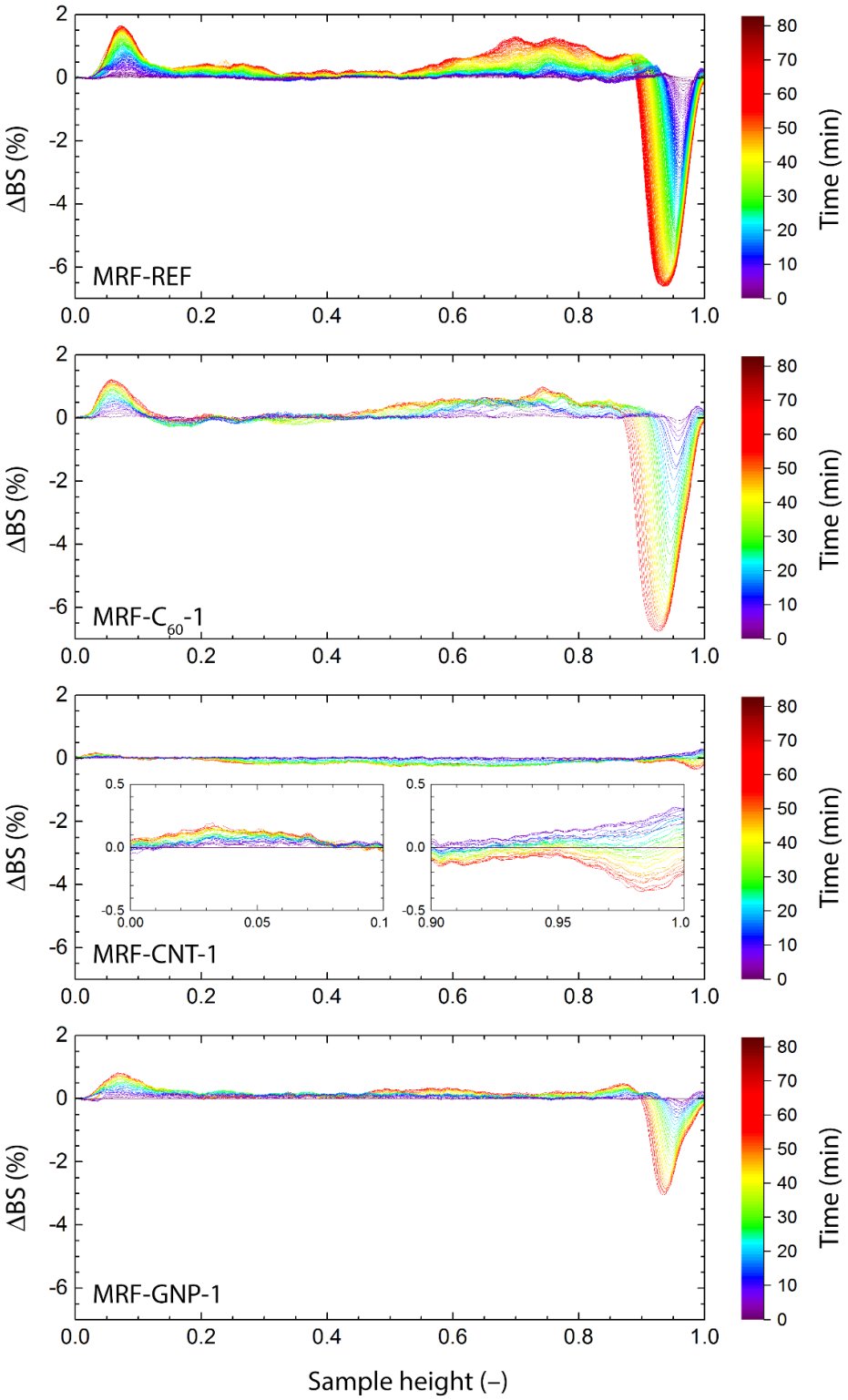

Figure 7. Turbiscan spectra of tested MRFs containing 60 wt.% of the CI particles and 1 wt.% of individual carbon additives. Insets in the MRF-CNT-1 spectrum show a sedimentation (*left*) and a clarification peak (*right*), respectively.

The Turbiscan® technology enables fast detection (typically less than hour) of all the destabilization phenomena (including clarification, sedimentation, agglomeration etc.) occurring in the samples during their aging [46]. Thus, one hour experiment was considered to be long enough to reliably assess and compare the sedimentation stability of the designed MRFs. In practice, the inactivity timespan can however reach several days (e.g. storage) [33] therefore the long-term experiment based on simple observation method was included. As can be seen in Figure 8, the MRF-C_{60}-1 exhibited similar stability when compared to the reference. The presence of small amount of fine C_{60} powder did not significantly affected the sedimentation process of the CI particles. Similar result was observed by Jang et al. [21] after adding the γ-Fe_2O_3 nanoparticles into the CI-based MRF. On the contrary, the presence of the GNPs slightly enhanced the suspension stability which was attributed to the plate-like morphology of the GNPs (Figure 1d). Considering the additive architecture, the GNPs most probably represented the spatial barriers decreasing the sedimentation velocity of the CI particles. Finally, the CNTs manifested as the most effective additive for the MRF stabilization. Their stabilization effect was caused by the buoyancy of the low-density additive particles [30] and is further closely-connected to relatively high off-state viscosity (Figure 2) of their suspensions. This type of behavior was recently observed on the electrorheological fluids containing the graphene oxide-wrapped titanium dioxide nanoparticles. Such additives act as a parachute that effectively prevents the dispersed particles from settling [47]. Finally, it should be mentioned that the naked eye observation can be interpreted as a subjective method from two main reasons. The first reason is connected to the opacity of the MRFs [30], while the second one appears because the macroscopic phase boundary between particle-rich phase and oil-rich one is not always sharply clarified. This phenomenon occurs as the particles do not sediment with the same velocities which stems from their size distribution. These drawbacks

can be eliminated using the inductance-based methods, which are at a stage of prototype development [30, 48]. However, direct observation is a sufficient method to establish the sample stability in a longer period of time and as demonstrated, the results were consistent with those obtained via Turbiscan method.

3.7 ***Redispersibility.*** Once the sedimentation occurs, the inter-particle aggregation is favored causing severe redispersibility problems [2]. However, despite its practical importance the redispersibility of the MRFs is rarely investigated [11, 26, 49]. This property can be enhanced by the use of the additives, which can eliminate direct contact of the CI particles leading to the effective prevention of rigid sedimentation cake occurrence during the long-term storage of the MRFs [37]. As shown in Figure 9, the CI particles exhibited good packing thus the height of the sedimentation cake was the lowest and the penetration force started to increase at the highest depth. The addition of fine C_{60} powder and GNPs slightly disturbed the packing properties of the CI, which was reflected in higher sediment, thus the penetration force increase at lower depth when compared with the reference. Finally, the CNTs cannot be easily structured, thus their presence prevented the packing of neighboring CI particles into stiff sedimentation cake. Therefore, the systems stabilized with the CNTs can be readily used after longer on-state inactivity when compared with the reference sample.

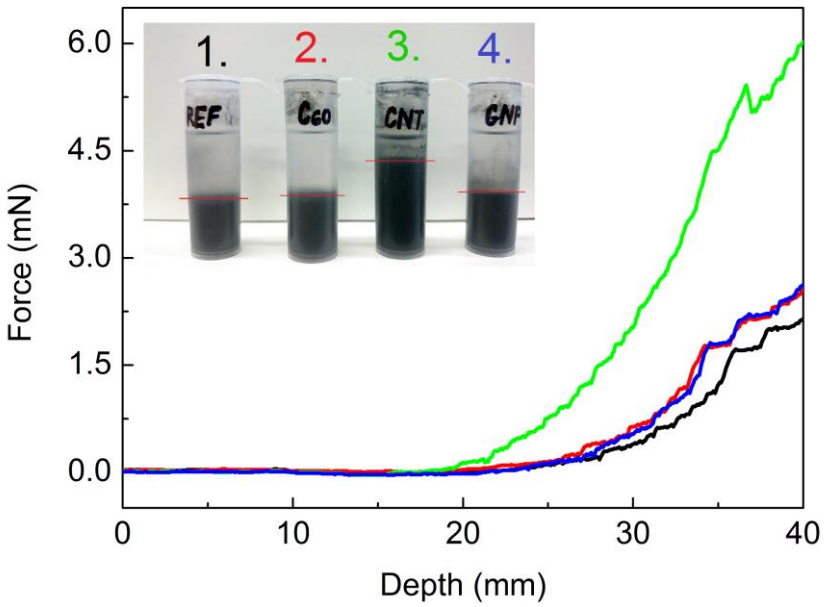

Figure 9. Penetration force as a function of depth for the reference sample (*black lines*), and the MRFs containing 1 wt.% of fine C_{60} powder (*red line*), the CNTs (*green line*), or the GNPs (*blue line*) measured on after 168-hour sedimentation. The inset shows the height of the sedimentation cake in the reference sample: 1; and the MRFs containing C_{60}, CNTs, and GNPs: 2, 3, and 4.

4. Conclusions

The effects of carbon additives on performance, stability and redispersibility of the magnetorheological fluids were investigated. It was found that fine fullerene powder added at low concentrations occupied the micro-cavities in the carbonyl iron field-induced structures possessing the noticeable reinforcing effect during magneto-steady shear. The presence of the carbon nanotubes and graphene nanoplatelets rather disrupted the chain-like structures, which was reflected in lower τ_0 and lower K parameter values. Due to introducing the carbon nanotubes into the system, the off-state τ_0 increased to the highest degree when compared with

other additives employed, which was further numerically quantified using the Robertson–Stiff model. Nevertheless, the Turbiscan characterization showed that the addition of carbon nanotubes remarkably enhanced sedimentation stability of the magnetorheological fluids, which was attributed to increased friction force as a result of their high specific surface area. The graphene nanoplatelets possessed only slight stabilizing effect. Finally, the fine fullerene powder and graphene nanoplatelets slightly disrupted the packing of the carbonyl iron particles after 168 hours of sedimentation. The carbon nanotubes appeared to be superior in this regard because they served as an effective additive, which prevents packing of the carbonyl iron particles resulting in the most stable magnetorheological fluids. Based on the results, it appears that the optimization of the magnetorheological fluid mixtures could be based on combining the additives varying in mechanism of their action (gap-filling and sedimentation enhancing effect) to ensure the both, rigidity of the internal structures as well as the sufficient sedimentation stability.

Acknowledgements

Author M. C. wishes to thank the Internal Grant Agency of Tomas Bata University in Zlin [project no. IGA/CPS/2017/004] for the financial support. This work was also supported by the Ministry of Education, Youth and Sports of the Czech Republic – Program NPU I [LO1504].

References

[1] M. Ashtiani, S.H. Hashemabadi, A. Ghaffari, A review on the magnetorheological fluid preparation and stabilization, Journal of Magnetism and Magnetic Materials, 374 (2015) 716-730.
[2] J. de Vicente, D.J. Klingenberg, R. Hidalgo-Alvarez, Magnetorheological fluids: a review, Soft Matter, 7 (2011) 3701-3710.

[3] W.L. Zhang, S.D. Kim, H.J. Choi, Effect of Graphene Oxide on Carbonyl-Iron-Based Magnetorheological Fluid, Ieee Transactions on Magnetics, 50 (2014) 4.
[4] Z. Strecker, I. Mazurek, J. Roupec, M. Klapka, Influence of MR damper response time on semiactive suspension control efficiency, Meccanica, 50 (2015) 1949-1959.
[5] J.D.G. Duran, G.R. Iglesias, A.V. Delgado, L.F. Ruiz-Moron, J. Insa, F. Gonzalez-Caballero, Stability and flow behavior of a magnetorheological lubricant in a magnetic shock absorber, Tribology Transactions, 51 (2008) 271-277.
[6] S.Q. Dai, C.B. Du, G.J. Yu, Design, testing and analysis of a novel composite magnetorheological fluid clutch, Journal of Intelligent Material Systems and Structures, 24 (2013) 1675-1682.
[7] D.M. Wang, Y.F. Hou, Z.Z. Tian, A novel high-torque magnetorheological brake with a water cooling method for heat dissipation, Smart Materials and Structures, 22 (2013) 11.
[8] W. Kordonski, A. Shorey, Magnetorheological (MR) jet finishing technology, Journal of Intelligent Material Systems and Structures, 18 (2007) 1127-1130.
[9] M. Cvek, M. Mrlik, M. Ilcikova, T. Plachy, M. Sedlacik, J. Mosnacek, V. Pavlinek, A facile controllable coating of carbonyl iron particles with poly(glycidyl methacrylate): a tool for adjusting MR response and stability properties, Journal of Materials Chemistry C, 3 (2015) 4646-4656.
[10] M. Sedlacik, V. Pavlinek, P. Saha, P. Svrcinova, P. Filip, J. Stejskal, Rheological properties of magnetorheological suspensions based on core-shell structured polyaniline-coated carbonyl iron particles, Smart Materials & Structures, 19 (2010) 6.
[11] M. Machovsky, M. Mrlik, T. Plachy, I. Kuritka, V. Pavlinek, Z. Kozakova, T. Kitano, The enhanced magnetorheological performance of carbonyl iron suspensions using magnetic Fe3O4/ZHS hybrid composite sheets, Rsc Advances, 5 (2015) 19213-19219.
[12] M. Mrlik, M. Ilcikova, M. Cvek, V. Pavlinek, A. Zahoranova, Z. Kronekova, P. Kasak, Carbonyl iron coated with a sulfobetaine moiety as a biocompatible system and the magnetorheological performance of its silicone oil suspensions, Rsc Advances, 6 (2016) 32823-32830.
[13] I.J. Moon, M.W. Kim, H.J. Choi, N. Kim, C.Y. You, Fabrication of dopamine grafted polyaniline/carbonyl iron core-shell typed microspheres and their magnetorheology, Colloids and Surfaces a-Physicochemical and Engineering Aspects, 500 (2016) 137-145.
[14] W.Q. Jiang, H. Zhu, C.Y. Guo, J.F. Li, Q. Xue, J.H. Feng, X.L. Gong, Poly(methyl methacrylate)-coated carbonyl iron particles and their magnetorheological characteristics, Polymer International, 59 (2010) 879-883.
[15] J. Sutrisno, A. Fuchs, H. Sahin, F. Gordaninejad, Surface Coated Iron Particles via Atom Transfer Radical Polymerization for Thermal-Oxidatively Stable High Viscosity Magnetorheological Fluid, Journal of Applied Polymer Science, 128 (2013) 470-480.
[16] M. Behrooz, J. Sutrisno, L.Y. Zhang, A. Fuchs, F. Gordaninejad, Behavior of magnetorheological elastomers with coated particles, Smart Materials and Structures, 24 (2015) 8.
[17] W.H. Chuah, W.L. Zhang, H.J. Choi, Y. Seo, Magnetorheology of Core-Shell Structured Carbonyl Iron/Polystyrene Foam Microparticles Suspension with Enhanced Stability, Macromolecules, 48 (2015) 7311-7319.
[18] M. Sedlacik, V. Pavlinek, R. Vyroubal, P. Peer, P. Filip, A dimorphic magnetorheological fluid with improved oxidation and chemical stability under oscillatory shear, Smart Materials and Structures, 22 (2013) 8.
[19] S.T. Lim, M.S. Cho, I.B. Jang, H.J. Choi, Magnetorheological characterization of carbonyl iron based suspension stabilized by fumed silica, Journal of Magnetism and Magnetic Materials, 282 (2004) 170-173.
[20] M.J. Hato, H.J. Choi, H.H. Sim, B.O. Park, S.S. Ray, Magnetic carbonyl iron suspension with organoclay additive and its magnetorheological properties, Colloids and Surfaces a-Physicochemical and Engineering Aspects, 377 (2011) 103-109.
[21] D.S. Jang, Y.D. Liu, J.H. Kim, H.J. Choi, Enhanced magnetorheology of soft magnetic carbonyl iron suspension with hard magnetic gamma-Fe2O3 nanoparticle additive, Colloid and Polymer Science, 293 (2015) 641-647.

[22] T. Plachy, M. Cvek, Z. Kozakova, M. Sedlacik, R. Moucka, The enhanced MR performance of dimorphic MR suspensions containing either magnetic rods or their non-magnetic analogs, Smart Materials and Structures, 26 (2017) 8.
[23] N. Jahan, S. Pathak, K. Jain, R.P. Pant, Enchancment in viscoelastic properties of flake-shaped iron based magnetorheological fluid using ferrofluid, Colloids and Surfaces A: Physicochemical and Engineering Aspects, 529 (2017) 88-94.
[24] S.H. Piao, M. Bhaumik, A. Maity, H.J. Choi, Polyaniline/Fe composite nanofiber added softmagnetic carbonyl iron microsphere suspension and its magnetorheology, Journal of Materials Chemistry C, 3 (2015) 1861-1868.
[25] M. Cvek, M. Mrlik, V. Pavlinek, A rheological evaluation of steady shear magnetorheological flow behavior using three-parameter viscoplastic models, Journal of Rheology, 60 (2016) 687-694.
[26] G.R. Iglesias, M.T. Lopez-Lopez, J.D.G. Duran, F. Gonzalez-Caballero, A.V. Delgado, Dynamic characterization of extremely bidisperse magnetorheological fluids, Journal of Colloid and Interface Science, 377 (2012) 153-159.
[27] F.F. Fang, Y.D. Liu, H.J. Choi, Y. Seo, Core-Shell Structured Carbonyl Iron Microspheres Prepared via Dual-Step Functionality Coatings and Their Magnetorheological Response, Acs Applied Materials & Interfaces, 3 (2011) 3487-3495.
[28] M. Mrlik, M. Ilcikova, M. Sedlacik, J. Mosnacek, P. Peer, P. Filip, Cholesteryl-coated carbonyl iron particles with improved anti-corrosion stability and their viscoelastic behaviour under magnetic field, Colloid and Polymer Science, 292 (2014) 2137-2143.
[29] M. Sedlacik, V. Pavlinek, A tensiometric study of magnetorheological suspensions' stability, Rsc Advances, 4 (2014) 58377-58385.
[30] G.R. Iglesias, A. Roldan, L. Reyes, L. Rodriguez-Arco, J.D.G. Duran, Stability behavior of composite magnetorheological fluids by an induction method, Journal of Intelligent Material Systems and Structures, 26 (2015) 1836-1843.
[31] G.R. Iglesias, L.F. Ruiz-Moron, J.I. Monesma, J.D.G. Duran, A.V. Delgado, An experimental method for the measurement of the stability of concentrated magnetic fluids, Journal of Colloid and Interface Science, 311 (2007) 475-480.
[32] X.G. Cao, H. Ren, H.Y. Zhang, Preparation and microwave shielding property of silver-coated carbonyl iron powder, Journal of Alloys and Compounds, 631 (2015) 133-137.
[33] M.A. Portillo, G.R. Iglesias, Magnetic Nanoparticles as a Redispersing Additive in Magnetorheological Fluid, Journal of Nanomaterials, (2017) 8.
[34] D.G. Zhao, J.A. Ning, S.Y. Li, M. Zuo, Synthesis and Thermoelectric Properties of C-60/Cu2GeSe3 Composites, Journal of Nanomaterials, (2016) 7.
[35] P. Filip, J. David, Axial Couette-Poiseuille flow of power-law viscoplastic fluids in concentric annuli, Journal of Petroleum Science and Engineering, 40 (2003) 111-119.
[36] M. Ashtiani, S.H. Hashemabadi, The effect of nano-silica and nano-magnetite on the magnetorheological fluid stabilization and magnetorheological effect, Journal of Intelligent Material Systems and Structures, 26 (2015) 1887-1892.
[37] S.H. Piao, W.L. Zhang, H.J. Choi, Magnetic Carbonyl Iron Suspension with Sepiolite Additive and Its Magnetorheological Property, Ieee Transactions on Magnetics, 50 (2014) 4.
[38] F.F. Fang, H.J. Choi, M.S. Jhon, Magnetorheology of soft magnetic carbonyl iron suspension with single-walled carbon nanotube additive and its yield stress scaling function, Colloids and Surfaces a-Physicochemical and Engineering Aspects, 351 (2009) 46-51.
[39] H.A. Barnes, The yield stress - a review or 'pi alpha nu tau alpha rho epsilon iota' - everything flows?, Journal of Non-Newtonian Fluid Mechanics, 81 (1999) 133-178.
[40] M.T. Balhoff, L.W. Lake, P.M. Bommer, R.E. Lewis, M.J. Weber, J.M. Calderin, Rheological and yield stress measurements of non-Newtonian fluids using a Marsh Funnel, Journal of Petroleum Science and Engineering, 77 (2011) 393-402.
[41] K.W. Song, Y.S. Kim, G.S. Chang, Rheology of concentrated xanthan gum solutions: Steady shear flow behavior, Fibers and Polymers, 7 (2006) 129-138.

[42] C. Galindo-Gonzalez, M.T. Lopez-Lopez, J.D.G. Duran, Magnetorheological behavior of magnetite covered clay particles in aqueous suspensions, Journal of Applied Physics, 112 (2012) 11.
[43] J.M. Ginder, L.C. Davis, Shear stresses in magnetorheological fluids - Role of magnetic saturation, Applied Physics Letters, 65 (1994) 3410-3412.
[44] D.H. Bae, H.J. Choi, K. Choi, J. Nam, M.S. Islam, N. Kao, Microcrystalline cellulose added carbonyl iron suspension and its magnetorheology, Colloids and Surfaces a-Physicochemical and Engineering Aspects, 514 (2017) 161-167.
[45] A. Peigney, C. Laurent, E. Flahaut, R.R. Bacsa, A. Rousset, Specific surface area of carbon nanotubes and bundles of carbon nanotubes, Carbon, 39 (2001) 507-514.
[46] H. Buron, O. Mengual, G. Meunier, I. Cayre, P. Snabre, Optical characterization of concentrated dispersions: applications to laboratory analyses and on-line process monitoring and control, Polymer International, 53 (2004) 1205-1209.
[47] X.F. Dong, S. Huo, M. Qi, Comparison of electrorheological performance between urea-coated and graphene oxide-wrapped core-shell structured amorphous TiO2 nanoparticles, Smart Materials and Structures, 25 (2016) 10.
[48] C. Galindo-Gonzalez, G.R. Iglesias, F. Gonzalez-Caballero, J.D.G. Duran, Stability of concentrated aqueous clay-magnetite suspensions, Colloids and Surfaces a-Physicochemical and Engineering Aspects, 306 (2007) 150-157.
[49] J.R. Morillas, A.J.F. Bombard, J. de Vicente, Preparation and characterization of magnetorheological fluids by dispersion of carbonyl iron microparticles in PAO/1-octanol, Smart Materials and Structures, 25 (2016) 10.

Supplementary Material

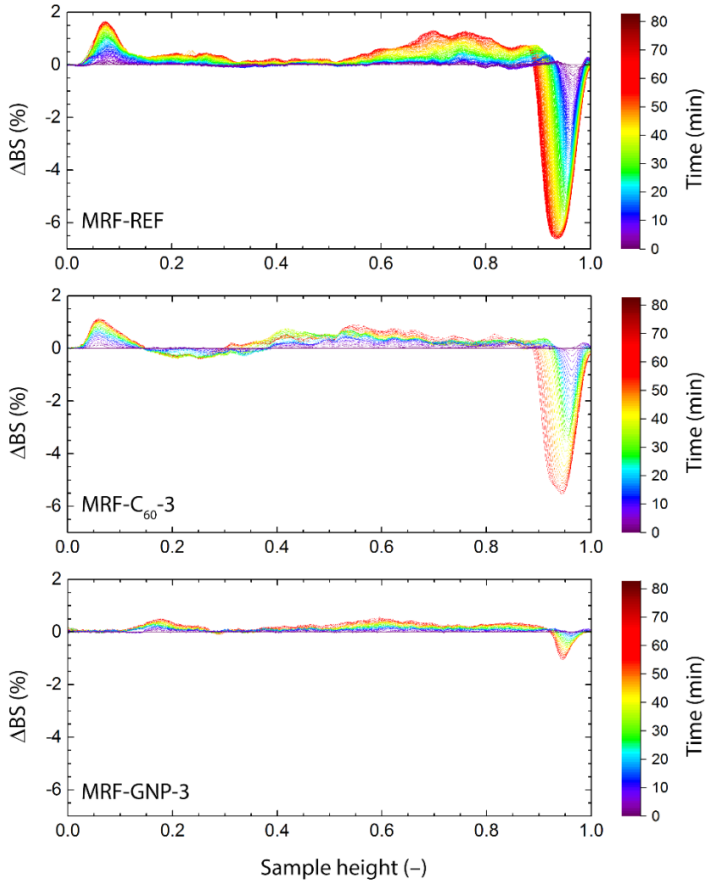

Figure S1. Turbiscan spectra of tested MRFs containing 60 wt.% of the CI particles and 3 wt.% of individual carbon additives.